Revista Brasileira de Aplicações de Vácuo, v. 23, n. 2, 76-81, 2004.

DESIGN AND CONSTRUCTION OF VACUUM SYSTEMS FOR LARGE AREA $CuIn_{1-x}Ga_xSe_{2-y}S_y$ THIN FILM SOLAR CELL FABRICATION

N.G. Dhere*; A.H. Jahagirdar; A.A. Kadam; S.S. Kulkarni; V.V. Hadagali; J.S. Shirolikar; M.W. Nugent
Florida Solar Energy Center, University of Central Florida
1679 Clearlake Road, Cocoa, FL 32922, U.S.A.

Received: October 20, 2004; Revised: November 25, 2004

Keywords: CIGS, vacuum system design, thickness uniformity

ABSTRACT

Two large-area vacuum systems have been designed, fabricated and installed to serve as a nucleus of a pilot plant for preparation of CIGS thin films solar cells. The chambers are pumped with cryopumps and rotary mechanical pump. The cryopumps are attached directly to the chambers through short tubulations and three-position gate valves because the cryopumps can operate in any orientation. The pumping speeds were chosen to obtain vacuum in the range of 10^{-5} Torr and 10^{-7} Torr in 5 minutes and 10 hours respectively. A graphical process has been developed and employed for representation of the variation of the rates of outgassing, throughput of vacuum pumps and the pressure with time. The vacuum chambers are fitted with five 10 cm x 30 cm magnetron sputtering sources for deposition of Mo, In, CuGa, ZnO, and ZnO:Al. Thickness uniformity over a large area (10 x 15 cm^2) was improved through adjustment of magnetic field by preferentially removing nickel-coated soft iron strips in the versatile magnetic array provided specifically for that purpose at the rear of the magnetron sputtering sources and by boosting the magnetic field at the extremities. CIGS Solar cells are being prepared routinely using these vacuum systems.

1. INTRODUCTION

$CuInSe_2$ (CIS) and $CuGaSe_2$, the materials that form the alloy $CuIn_{1-x}Ga_xSe_{2-y}S_y$ (CIGS), belong to the semiconducting I-III-VI_2 materials family that crystallize in the tetragonal chalcopyrite structure (Figure 1). CIGS thin film solar cells have the highest efficiencies amongst all the thin film solar cells [1, 2]. The record efficiencies for small CIGS solar cells and minimodules are 19.5% by National Renewable Energy Laboratory (NREL), USA and 16.6% by Angstrom Solar Center, Uppsala, Sweden. Record CIGS module efficiencies are 12.8% by Shell Solar, USA, 12.8 Showa Shell, Japan, 13% Würth Solar, Germany and 13.1% Shell Solar, Germany [1].

CIGS solar modules are expected to become cheaper than crystalline silicon modules within this decade. Non-availability of turn-key facilities is one of the major factors impeding the introduction of economic, large-scale CIGS thin-film PV module manufacture. Therefore, the design, operation and control facilities for large-scale manufacture must be custom-built. Very few research laboratories are conducting research on development of photovoltaic (PV) plants. The effort presented in this paper is an attempt to fulfill this lacuna.

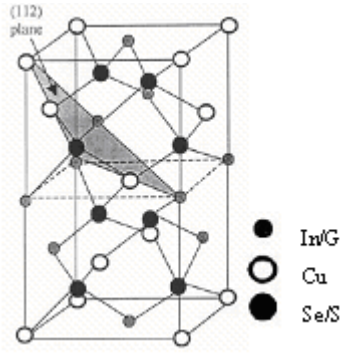

Figure 1 – Chalcopyrite structure.

CIGS Thin-film solar cells are being prepared routinely at Florida Solar Energy Center (FSEC) PV Materials Lab on glass for terrestrial substrates and on flexible metallic foils for space applications. The configuration of CIGS cells is substrate/Mo/CIGS/CdS/ZnO/ZnO:Al/Ni-Al (Figure 2). Cell preparation is carried out in two stages, (i) deposition of molybdenum back contact and CuGa/In metallic precursors on glass or flexible metallic foil substrate by DC magnetron sputtering and (ii) selenization/sulfurization of CuGa/In metallic precursors in diethylselenide (DESe) and H_2S atmosphere to get p-type CIGS thin films. The CIGS thin film solar cells are completed by the deposition of n-type CdS heterojunction partner layer using chemical bath deposition (CBD), ZnO/ZnO:Al transparent conducting oxide bilayer by RF magnetron sputtering and Ni-Al front contacts by e-beam evaporation [3,4].

2. SPUTTERING SYSTEM DESIGN

Earlier thin film deposition at the FSEC PV Materials Lab was carried out on 3 x 3 cm^2 substrates in a large vacuum chamber having diameter of 45.7 cm and height of 376.2 cm, using DC magnetron sputtering and a small 15 cm diameter six-way cross chamber using RF magnetron sputtering. Deposition parameters were optimized for achieving

* dhere@fsec.ucf.edu

high-efficiency solar cells on glass and flexible metallic foil substrates. An efficiency of 10.4% was achieved for a small (0.42 cm^2) $Cu(In,Ga)S_2$/CdS thin film solar cell on 3 x 3 cm^2 stainless steel substrate [3]. More recently, two large-area sputtering systems have been developed for preparation of CIGS thin-film solar cells for terrestrial and space applications on large (15 x 10 cm^2) substrates with the aim of establishing a pilot plant size facility. The equipment would be capable of carrying out roll-to-roll deposition on 15-cm width with minor modifications. A pilot plant size selenization/sulfurization furnace received as donation from Siemens Solar (presently Shell Solar) Industries has been installed. It can accommodate one hundred 10 x 10 cm^2 or sixty-six 15 x 10 cm^2 size substrates. It may be noted that substrate width in large scale manufacturing plants is 60 cm. Thus the experience on process optimization gained through this equipment will be applicable to a manufacturing plant relatively easily.

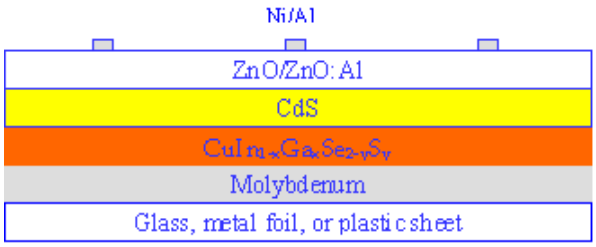

Figure 2 – Cell configuration of CIGSS/CdS thin film solar cell.

The two large-area sputtering systems have been designed, fabricated and installed. The internal dimensions of vacuum chambers of the two systems are 97.8 cm x 46.99 cm x 15.24 cm and 67.3 cm x 46.99 cm x 15.24 cm. High Vacuum is obtained in the larger and smaller chambers with cryopumps having pumping speeds of 1500 liters/second and 800 liters/second. The cryopumps are attached directly at the rear of the larger and smaller chambers through 11.43 cm diameter and 6.35 cm long tubulations and pneumatic three-position gate valves having openings of diameters of 20 cm and 15 cm respectively (Figures 3, 4 a, b and 5 a, b). It was possible to connect the cryopumps through such a short tubulation because of the fact that a cryopump can operate in any orientation. Rough vacuum is obtained in the two vacuum systems with two-stage rotary mechanical pumps both having a pumping speed of 340 liters/minute. Both are attached to the vacuum chambers through tubulations and pneumatic valves having a diameter 3.81 cm and total length of 121.9 cm. Each system is equipped with mass-flow controllers, convectron and Bayard-Alpert ionization gauges, and feed-thru's for "in situ" diagnostic tools.
The larger vacuum system having a chamber with the external dimensions 99 cm x 49.53 cm x 18.4 cm is fitted with three 10 cm x 30 cm DC magnetron sputtering sources for deposition of molybdenum, indium, and CuGa (22 atomic %) thin films (Figure 4a and 4b) and a smaller system having a chamber with the external dimensions 72 cm x 49.53 cm x 18.54 cm is fitted with two 10 cm x 30 cm RF magnetron sputtering sources for deposition of transparent and conducting ZnO and ZnO:Al bilayer window layers (Figure 5a and 5b).

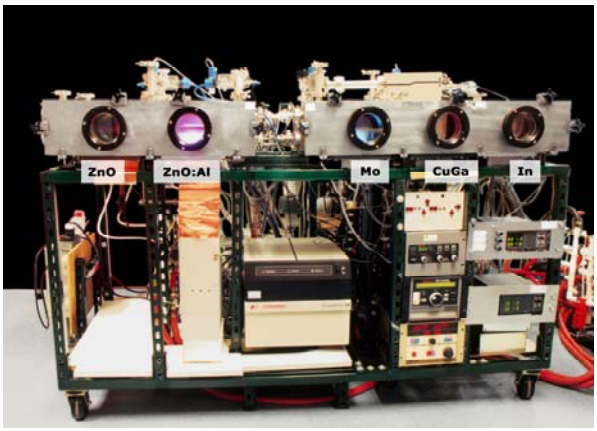

Figure 3 – Large area magnetron sputtering unit.

The width and the length of chambers were determined based on the size of the sputtering sources (10x30 cm^2) and height was determined based on the optimum distance between substrate and the sputtering target (~7.5 cm). Substrates were moved in a linear fashion along the 10-cm width of the sputtering target to improve thickness uniformity along that direction. A computer-controlled linear substrate motion mechanism was designed, constructed and installed for this purpose. It is driven by a stepper motor for precise control of the linear motion. Thickness uniformity along the 30-cm length of the sputtering target was improved through adjustment of magnetic field by preferentially removing nickel-coated soft iron strips in the versatile magnetic array provided specifically for that purpose at the rear of the magnetron sputtering sources. The process to achieve high thickness uniformity over an area of 10 x 15 cm^2 is described in Section 2.2.

2.1 DESIGN CALCULATIONS

A rotary mechanical pump having a pumping speed of 340 liters/minute was used for obtaining a rough vacuum of ~$5x10^{-2}$ Torr from atmospheric pressure, p_0. Vacuum pumping calculations were carried out by dividing this pressure range in two sub regimes, viz. viscous flow regime from 760 Torr till ~7.6 Torr and slip flow regime from 7.6 Torr to ~ $5x10^{-2}$ Torr.

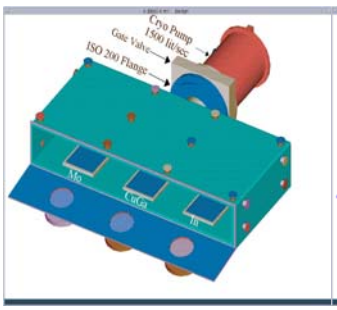

Figure 4a – Larger chamber solid model

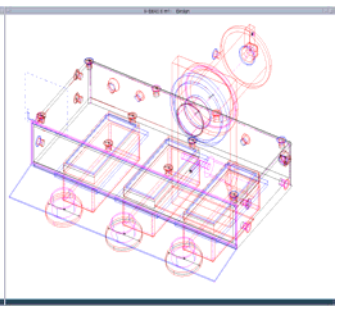

Figure 4a – Larger chamber wire frame model.

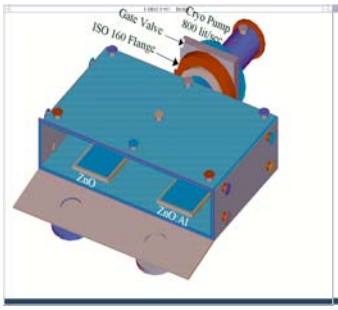

Figure 5a - Smaller chamber solid model.

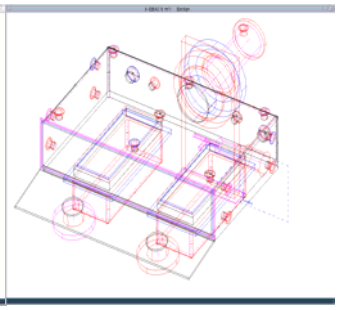

Figure 5b - Smaller chamber wire frame model.

(i) Viscous Flow Regime: The time, t for pumping from atmospheric pressure, p_0 to intermediate pressure, p of ~7.6 Torr is given by equation 1 [5]. Here the effective pumping speed, S_{eff}, is calculated using equation 2, by inserting pumping speed, S_p of the rotary mechanical pump and conductance, C of the roughing line [5]. Here the conductance C of the roughing line is calculated using equation 3 for the viscous flow regime where P_{av} is the average pressure and D and L are the diameter and length of the roughing line respectively [5]. For both the chambers, the pumping speed of the rotary mechanical pump, S_p is 340 liters/minute while the diameter, D and total length, L of the roughing line are 3.81 cm and 121.9 cm respectively.

The conductance, C and effective pumping speed, S_{eff} calculated using equations 2 and 3 were 6.96 x 10^6 liters/minute and 340 liters/minute respectively for both the chambers. Calculations using equation 1, showed that it would take 57 seconds to attain the pressure of 7.6 Torr for larger chamber having volume, V of 70 liters and 39 seconds for the smaller chamber having volume, V of 48.2 liters.

$$t = \frac{V}{S_{eff}} \ln \frac{p_0}{p} \quad (equation\ 1)$$

$$\frac{1}{S_{eff}} = \frac{1}{C} + \frac{1}{S_p} \quad (equation\ 2)$$

$$C = 1.34 \times 10^3 \times D^4 \frac{\bar{p}}{L} \quad (equation\ 3)$$

(ii) Slip Flow Regime: For pumping from 7.6 Torr to ~ $5x10^{-2}$ Torr, in the slip flow regime, the conductance, C of the roughing line is give by equation 4 (5).

$$C = C_m \left[0.0736 \frac{D}{\lambda} + \frac{1+1.253\frac{D}{\lambda}}{1+1.547\frac{D}{\lambda}} \right] \quad (equation\ 4)$$

where, λ/D is Knudsen number, K, and molecular flow conductance of a long tube, C_m is given by:

$$C_m = C_0 \frac{4D}{3L} \quad (equation\ 5)$$

Here the entrance conductance, C_0 is given by:

$$C_0 = \frac{v_{av}}{16} \pi D^2 \quad (equation\ 6)$$

where the value of mean velocity, v_{av} of air at 20°C is 464.2 m/s [5].

The mean free path, λ for air at a pressure of $5x10^{-2}$ Torr is 10^{-3} m. Therefore, the value of Knudsen number, K becomes 0.0262. Using these values, the entrance conductance, C_0, flow conductance, C_m, conductance, C and effective pumping speed, S_{eff} were calculated to be 0.1323 m^3/s, $5.514x10^{-3}$ m^3/s, 1197 liters/minute and 265 liters/minute respectively. Therefore, it would take 1 minute and 20 seconds to attain the pressure of ~$5x10^{-2}$ Torr from ~7.6 Torr in the larger chamber and 55 seconds for the smaller chamber. Moreover, the total time to obtain rough vacuum of ~$5x10^{-2}$ Torr from atmospheric pressure will be 2 minutes and 17 seconds for larger chamber and 1 minutes and 34 seconds for smaller chamber.

Most important flow regimes are the extreme ones of viscous or continuum flow and molecular flow since they cover the most extensive ranges under practical conditions. For most purposes, it is sufficient to limit calculation of systems to those two regimes and consider the slip regime as simple transition and variation near these two limits. It may be noted that the cut-off for changing from pumping with a rotary mechanical pump to that with cryopump of $5x10^{-2}$ Torr has been chosen to be considerably higher than the ultimate vacuum of the mechanical pump so as to minimize backstreaming of pump fluid vapors as well as to maintain the pumping speed near the geometrical pumping speed.

(iii) Molecular Flow Regime: As mentioned above, high vacuum is obtained in the larger and smaller chambers with cryopumps having pumping speeds of 1500 liters/second and 800 liters/second and that a tubulation of D = 0.1143 m and L = 0.0635 m is used to connect the cryopumps to both the chambers. Also for the larger chamber, a gate valve opening is 0.2 m and for the smaller chamber a gate valve opening is 0.15 m. The conductances C_1 and C_2 of the tubulation and gate valve opening respectively were calculated using equation 7 (5).

$$C = 116AW \quad (equation\ 7)$$

where, A is area at the entrance and W is transmission probability for circular tubes obtained from Holland et al [5].

The conductance of the tubulation, C_1 for the both the chambers was calculated to be 0.7998 m^3/s. The conductances, C_2 of the gate valves for the larger and smaller chambers were calculated to be 2.45 m^3/s and 1.37 m^3/s respectively.

The total conductance C of the tubulation in series with the gate valve is given by equation 8.

$$\frac{1}{C} = \frac{1}{C_1} + \frac{1}{C_2} \quad (equation\ 8)$$

The total conductances C of the tubulation in series with the gate valve for the larger and smaller chambers were calculated to be 0.603 m^3/s and 0.506 m^3/s respectively. Therefore, the effective pumping speeds of cryopumps having pumping speed of 1500 liters/second and 800 liters/second respectively for the larger and smaller chamber calculated using equation 2 were 0.43 m^3/s and 0.3099 m^3/s respectively.

Additionally, the area of the internal walls together with that of the accessories (typically 50% of that of the walls) for the larger vacuum chamber having the dimension 97.8 cm x 46.99 cm x 15.24 cm and smaller vacuum chamber having the dimension 67.3 cm x 46.99 cm x 15.24 cm are respectively 2.04 m^2 and 1.4714 m^2. The chambers and the accessories are mostly made of stainless steel. The outgassing rate per unit area, Q, of stainless steel is initially $3x10^{-4}$ Pa m^3 per second per m^2 (5). Therefore, the initial total outgassing rates of the two chambers are $6.12x10^{-4}$ Pa m^3 per second and $4.414x10^{-4}$ Pa m^3 per second respectively. The outgassing rate will fall at a rate of $1/t^a$ where 'a' has a value between 0.7 and 2 (5). In the case of stainless steel it has been estimated to be 1.06.

The throughput of a pump having an effective pumping speed, S_{eff} at a pressure, P is S_{eff} x P. It may be noted that there is a dynamic equilibrium between the outgassing rate and throughput of the pump. Therefore, the vacuum chamber having a total instantaneous outgassing rate of Q would attain instantaneous pressure, P of Q/S_{eff}, if it is reasonably free of real leaks. In fact, the rate of real leaks of both the chambers after thorough testing with a mass spectrometer leak detector were found to be below 10^{-7} Pa m^3 per second.

Figures 6a and 6b show graphic representation of the calculations of the instantaneous outgassing rates and system pressure with time of pumping, t in hours. It can be used to determine the pressure after a given time of pumping or alternatively the time necessary to achieve a desired pressure. Thus the instantaneous pressures of the larger chamber at the beginning, after 5 and 10 hours would be $1.07x10^{-5}$, $1.85x10^{-6}$ and $3.21x10^{-7}$ Torr. Similarly, for the smaller chamber, the instantaneous pressures at the beginning, and after 5 and 10 hours would be $1.07x10^{-5}$, $1.86x10^{-6}$ and $3.22x10^{-7}$ Torr.

The total leakage rate, Q_{total} is given by the sum of the real leakage rate and virtual leakage rate i.e. the outgassing rate.

Tables 1 and 2 provide the total leakage rates, Q_{total} and pressures at the beginning and after 5 Hrs and 10 Hrs for the larger and smaller chambers.

In fact, the actual initial high vacuum attained in both the chambers was ~$1x10^{-5}$ Torr while high vacuum of <$5x10^{-6}$ Torr and >$5x10^{-7}$ Torr were obtained respectively after pumping for a few hours and after overnight pumping.

It may be noted that the fabrication cost of the two large-area sputtering systems was 35-40% of standard commercial equipment while at the same time they are more appropriate for the cell preparation process.

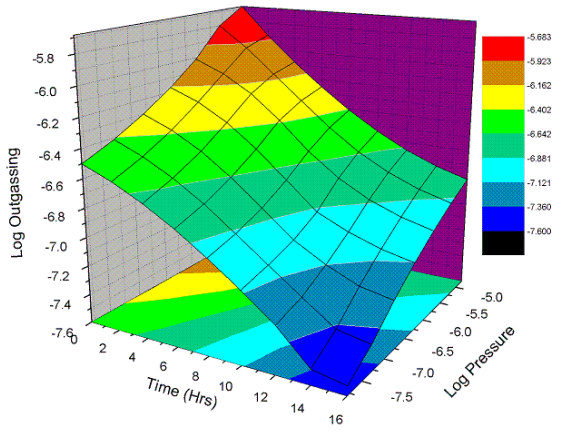

Figure 6b - Graph of time Vs Log Pressure Vs log outgassing for smaller chamber.

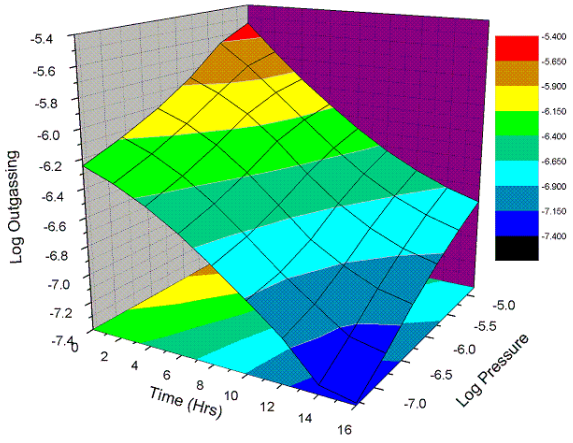

Figure 6a - Graph of time Vs Log Pressure Vs log out gassing for larger chamber.

Table 1 - Total Leakage Rates and Pressures of the Larger Chamber

	Q_{total} (Torr m^3/s)	Pressure (Torr)
Beginning	$4.60x10^{-6}$	$1.07x10^{-5}$
5 Hrs	$7.975x10^{-7}$	$1.85x10^{-6}$
10 Hrs	$1.38x10^{-7}$	$3.21x10^{-7}$

Table 2 -Total Leakage Rates and Pressures of the Smaller Chamber

	Q_{total} (Torr m^3/s)	Pressure (Torr)
Beginning	$3.3188x10^{-6}$	$1.07x10^{-5}$
5 Hrs	$5.75x10^{-7}$	$1.856x10^{-6}$
10 Hrs	$9.968x10^{-8}$	$3.217x10^{-7}$

2.2 THICKNESS UNIFORMITY

Experimentation for improvement of thickness uniformity was carried out by depositing individual molybdenum and zinc oxide thin films on large-area glass substrates using optimized parameters of DC or RF sputtering power, working gas pressure, target-to-substrate distance, sputtering time and linear substrate movement parallel to the 10-cm width of the target.

Prior to the deposition of molybdenum and zinc oxide layers, a square grid pattern was drawn on clean, 10 cm x 15 cm glass substrates using a permanent marker. After the depositions of individual molybdenum or zinc oxide films, the grid pattern together with the overlaying thin film was removed by ultrasonic cleaning in isopropanol. This provided a distinct step for measurements with a Dektak[3] thickness profilometer. Initially, a thickness variation of ±11% region was observed over the central 10 x 10 cm^2 area. Series of experiments were carried out for improvement in thickness uniformity by empirically modifying the magnetic field distribution by selectively removing nickel-coated soft iron strips specifically provided at the rear of the magnetron sputtering sources for this purpose. The strips were replaced by similar-size rubber strips to maintain the shape integrity. The optimum configuration was determined after experimenting with various permutations and combinations of nickel coated soft iron strips arrangements. It resulted in a thickness uniformity of ±3% over central 10x10 cm^2 region for molybdenum thin films (Figure 7) while the thickness continued to drop precipitously beyond this region. The precipitous drop in thickness beyond 10 cm was attributed to drop in the magnetic field at the extremities. It was, therefore, decided to boost the magnetic field at the extremities to achieve better thickness uniformity. The sputtering sources were also found to produce non-uniform plasma distribution within the racetrack leading to varying plasma intensity glow, again confirming the need to modify magnetic array.

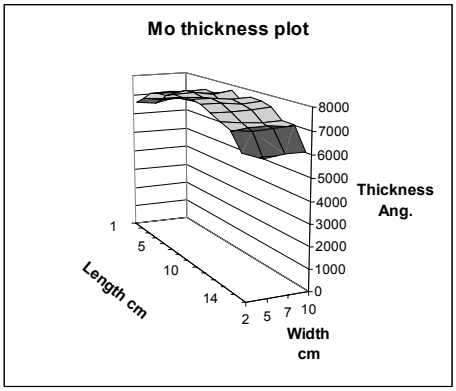

Figure 7 -Thickness distribution profile.

In the mean time, the manufacturer had modified the magnetic array with a better magnetic field distribution and stronger magnetic field at the extremities. Two such new magnetron-sputtering sources were procured. The design introduced extra magnets at and near the periphery. The three old magnetron-sputtering sources were modified to match the new magnetic array design with additional magnets obtained from the manufacturer. For this purpose, the copper body holding the magnetic assembly was machined to accommodate the modified assembly. The problem of non-uniform plasma was resolved after modifying magnetic assembly. The initial non-uniform plasma was modified into the dumbbell shape of the racetrack region with the modified magnetic arrays that have stronger magnetic field at extremities (Figure 8a and 8b).

Figure 9 shows variation of thicknesses of molybdenum and zinc oxide deposited respectively by DC and RF magnetron sputtering averaged over 7 cm distances along the linear movement direction with the length parallel to the 30-cm dimension of sputtering sources.

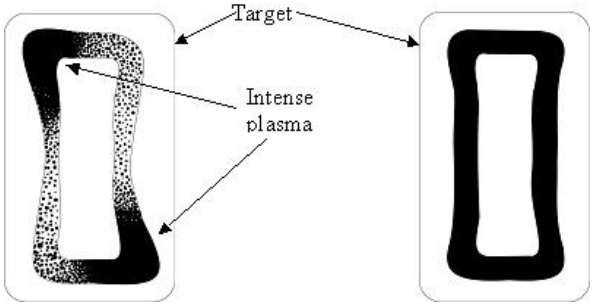

Figure 8a -Non-uniform plasma. **Figure 8b - Uniform plasma.**

The thickness uniformities over central lengths were: Molybdenum: ±2.24 % over 10 cm, ±2.40% over 12.7 cm, ±2.95% over 15.2cm and zinc oxide: ±2.46 % over 10 cm, ±3.84% over 12.7 cm, ±5.60% over 15.2 cm. Fortunately the thickness uniformity for ZnO/ZnO:Al is slightly less critical in the preparation of CIGS thin film solar cells. These results pave the way for deposition of large area (15 cm x 10 cm) thin film solar cells.

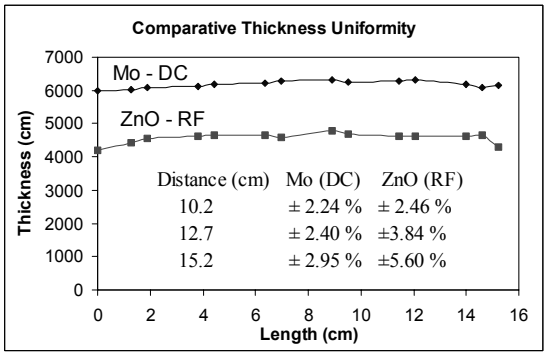

Figure 9 - Thickness variation plots Mo (DC sputtering) and ZnO (RF sputtering).

Figure 10 shows a large number of small thin film solar cells prepared on 10 cm x 10 cm stainless steel foil at FSEC PV Materials lab.

3. CONCLUSION

Two large area magnetron sputtering units have been designed, fabricated and installed. A selenization/sulfurization furnace, H_2S/H_2Se scrubber for the furnace, chemical bath deposition system for CdS deposition and e-beam evaporation systems have also been installed and are being used routinely for the preparation of CIGS thin films on large (15 cm x 15 cm) substrates and solar cells on 10 cm x 10 cm substrates.

The fabrication cost of the equipment was 35-40% of standard commercial equipment while at the same time, designed equipment is more appropriate for the cell preparation process.
The experience on process optimization gained through this equipment can be applied to a large-scale manufacturing plant relatively easily.

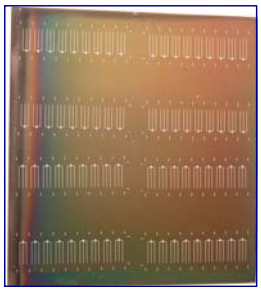

Figure 10 - Thin film solar cell prepared at FSEC PV Materials Lab on SS foil

ACKNOWLEDGEMENT

The authors would like to acknowledge the funding for this research from the National Renewable Energy Laboratory, the NASA Glenn Research Center, and University of Central Florida Presidential Funding for Equipment.

REFERENCES

1. ULLAL, H., *Polycrystalline Thin-Film Photovoltaic Technologies: Progress And Technical Issues*, Proceedings of the 14th Photovoltaic Science and Engineering Conference, Bangkok, Thailand (2004) 417.
2. RAMANATHAN, K.; CONTRERAS, M.A.; PERKINS, C.L.; ASHER, S.; HASOON, F.S.; KEANE, J.; YOUNG, D.; ROMERO, M.; METZGER, W.; NOUFI, R.; WARD, J.; DUDA, A., *Prog. Photovolt: Res. Appl.* 11 (2003) 225–230.
3. DHERE, N.G.; GADE, V.S.; JAHAGIRDAR, A.H.; KADAM, A.A.; PATIL, H.P.; KULKARNI, S.S., *J. Vac. Sci. Technol. (A)* 21 (2003) 1442-1446.
4. DHERE, N.G.; GHONGADI, S.R.; PANDIT, M.B.; JAHAGIRDAR, D.A.H., *Prog. Photovolt: Res. Appl.* 10 (2002) 407-416.
5. HOLLAND, L.; STECHELMAYER, A.; YARWOOD, J.; (Ed.s), *Vacuum Manual*, E. & F. N. Spon, London, (1974).